Biomass burning aerosol absorption measurements with MODIS using the critical reflectance method

L. Zhu,[1] J. V. Martins,[1] and L. A. Remer[2]

Received 13 October 2010; revised 23 January 2011; accepted 3 February 2011; published 9 April 2011.

[1] This research uses the critical reflectance technique, a space-based remote sensing method, to measure the spatial distribution of aerosol absorption properties over land. Choosing two regions dominated by biomass burning aerosols, a series of sensitivity studies were undertaken to analyze the potential limitations of this method for the type of aerosol to be encountered in the selected study areas, and to show that the retrieved results are relatively insensitive to uncertainties in the assumptions used in the retrieval of smoke aerosol. The critical reflectance technique is then applied to Moderate Resolution Imaging Spectrometer (MODIS) data to retrieve the spectral aerosol single-scattering albedo (SSA) in South African and South American biomass burning events. The retrieved results were validated with collocated Aerosol Robotic Network (AERONET) retrievals. Approximately 67% of the comparisons show a difference between MODIS and AERONET smaller than 0.03, the magnitude of the AERONET uncertainty. The overlap of the two retrievals increases to 88%, allowing for measurement variance in the MODIS retrievals, as well. The ensemble average of MODIS-derived SSA for the Amazon forest station is 0.92 at 670 nm, and 0.84–0.89 for the southern African savanna stations. The critical reflectance technique allows evaluation of the spatial variability of SSA and shows that SSA in South America exhibits higher spatial variation than in South Africa. The accuracy of the retrieved aerosol SSA from MODIS data indicates that this product can help to better understand how aerosols affect the regional and global climate.

Citation: Zhu, L., J. V. Martins, and L. A. Remer (2011), Biomass burning aerosol absorption measurements with MODIS using the critical reflectance method, *J. Geophys. Res.*, *116*, D07202, doi:10.1029/2010JD015187.

1. Introduction

[2] Atmospheric aerosols absorb solar radiation, warm the atmosphere [*Penner et al.*, 1992], and cool the Earth surface [*Ramanathan et al.*, 2001]. Therefore, they disturb the atmospheric temperature profile [*Ackerman et al.*, 2000; *Ramanathan et al.*, 2007; *Davidi et al.*, 2009], and affect cloud properties [*Koren et al.*, 2004, 2008; *Feingold et al.*, 2005] and precipitation [*Ramanathan et al.*, 2001, 2005; *Menon et al.*, 2002]. These effects are particularly important over areas with high aerosol concentration [*Sato et al.*, 2003; *Wang*, 2004], such as the southern Africa region [*Ichoku et al.*, 2003], the Amazon region [*Procopio et al.*, 2004], the Asian region [*Ramana and Ramanathan*, 2006], and Yellow Sea, Arabian Sea, and Saharan Coast region [*Zhu et al.*, 2007]. A quantitative understanding of the role of absorbing aerosols in climate change is also required to formulate reliable policy recommendations [*Hansen et al.*, 2000].

[3] Aerosol absorption is typically expressed in terms of aerosol single-scattering albedo ($SSA = \frac{\text{aerosol scattering coefficient}}{\text{aerosol scattering coefficient} + \text{aerosol absorption coefficient}}$). The importance of aerosol SSA to climate change was first studied back in the 1970s [*Atwater*, 1970; *Mitchell*, 1971]. However, even though SSA is the biggest contributor to the total uncertainty in aerosol direct radiative forcing [*McComiskey et al.*, 2008], accurate aerosol SSA retrieval remains challenging still today [*Heintzenberg et al.*, 1997; *Moosmüller et al.*, 2009]. Many approaches have been developed to study aerosol absorption properties, including microphysical simulations [*Ackerman and Toon*, 1981; *Martins et al.*, 1998], data analysis from AERONET [*Dubovik et al.*, 2002], and in situ measurements [*Clarke et al.*, 1967; *Hansen et al.*, 1984; *Reid et al.*, 1998; *Bond et al.*, 1999; *Martins et al.*, 2009], and ground-based remote sensing techniques [*Dubovik et al.*, 1998]. Space-based remote sensing techniques to measure aerosol absorption have also been increasingly developed. More specifically, TOMS and combination of multisensors on different satellites have been used to study aerosol absorption. However, the retrieval of SSA from TOMS is limited in the UV range (320–440 nm), and the result is sensitive to the assumed aerosol layer height [*Herman et al.*, 1997; *Torres et al.*, 1998]. Moreover, the combination of satellite sensors, such as TOMS and ERBE

[1]Department of Physics, Joint Center for Earth Systems Technology, University of Maryland, Baltimore County, Baltimore, Maryland, USA.
[2]NASA Goddard Space Flight Center, Greenbelt, Maryland, USA.

Copyright 2011 by the American Geophysical Union.
0148-0227/11/2010JD015187

[*Hsu et al.*, 2000], TOMS and MODIS [*Hu et al.*, 2007], OMI and MODIS [*Satheesh et al.*, 2009], TOMS, MODIS and MISR [*Hu et al.*, 2009], and A-train satellite sensors (MODIS, OMI, and CALIPSO) [*Jeong and Hsu*, 2008], have been used to retrieve SSA. Nevertheless, these retrievals are still limited to the UV range, and the error sources introduced by using multiplatforms with different resolutions, slightly different observation times, and different calibrations have not yet been well studied.

[4] Recently, some other space-based techniques have been proposed to study aerosol absorption as well. Measuring aerosol SSA over ocean from space, by using ocean sun glint as a bright background against aerosol absorption, was proposed by *Kaufman et al.* [2002]. MISR also has the ability to distinguish weakly absorbing (having 1–4% of hematite, SSA in the range of 0.98–0.99) and strongly absorbing (having 10% hematite, red channel SSA of about 0.94) dust components [*Kalashnikova et al.*, 2005; *Kalashnikova and Kahn*, 2006]. Moreover, on the basis of the fact of differing sensitivities of polarized and unpolarized reflectance to aerosol absorption, Glory will be used to retrieve SSA from polarimetric measurements in a single pixel [*Mishchenko et al.*, 2007, Table 2]. Even with these efforts, however, aerosol absorption measurement with satellite remote sensing still remains challenging and more studies are needed.

[5] Compared with the techniques discussed above, the "critical reflectance" method is also a promising space-based remote sensing technique to retrieve SSA [*Fraser and Kaufman*, 1985]. According to the *Fraser and Kaufman* [1985] radiative transfer simulations, there exists a specific surface reflectance for which increased aerosol loading (being represented here by aerosol optical depth (AOD)) does not change the reflectance at the top of the atmosphere (TOA). This unchanging reflectance at the TOA is defined as the critical reflectance, which has a one-to-one relationship to aerosol SSA [*Fraser and Kaufman*, 1985]. This technique has been utilized with several space-based remote sensing instruments to retrieve aerosol SSA: (1) using Landsat MultiSpectral Sensor Imagery as well as aircraft radiance data to retrieve aerosol SSA over the DC area [*Kaufman*, 1987]; (2) using AVHRR images in visible and near-IR bands to retrieve the SSA of forest smoke [*Kaufman et al.*, 1990]; (3) using Landsat TM images to retrieve dust SSA, where the result agreed well with AERONET SSA [*Kaufman et al.*, 2001].

[6] This research applies the critical reflectance technique to MODIS data to retrieve aerosol SSA. The first MODIS sensor aboard NASA's Terra satellite was launched in 1999 and the second one on the Aqua satellite launched in 2002. Each MODIS sensor provides a global data set every 1–2 days with a 16 day repeat cycle. The sensors collect the Earth images at 36 spectral bands in the wavelength range from 0.4 to 14.4 μm with a swath width of 2330 km (cross track) and continuous along-track coverage. Specifically, the seven aerosol bands are: 0.62–0.67, 0.84–0.87, 0.46–0.48, 0.55–0.57, 1.2–1.3, 1.63–1.65, and 2.11–2.16 μm, nominally 0.67, 0.86, 0.47, 0.55, 1.24, 1.64, and 2.12 μm, respectively. Like any other retrievals and measurements having limitations, the application of this algorithm is limited by cloud coverage, satellite geometry, AOD difference between the polluted and clean days, and other factors that are discussed here as part of our sensitivity studies. These limitations may impact the global applicability of the method but the method still produces valuable measurements of single-scattering albedo in many locations around the globe. This research discusses how to calculate the critical reflectance from MODIS data and the sensitivity of potential factors affecting the retrieval, such as detector zenith angle (DZA) and AOD difference between the polluted day and the clean days. We also present validation results with collocated AERONET measurements as well as regional SSA and aerosol absorption optical depth (AAOD) maps.

2. Measuring Critical Reflectance From MODIS Data and Retrieving Aerosol SSA

[7] In this section, we use 2 days of MODIS images 16 days apart at the AERONET Mongu site (latitude = −15.25°, longitude = 23.15°) with low AOD (0.36 at 0.67 μm) day 266 and high AOD (0.7 at 0.67 μm) day 250 in year 2000 to describe how to calculate the critical reflectance parameter. The 16 days apart are used to assume the same angular geometry. In the rest of this study, we will refer to the low AOD day as the "clean day" and the high AOD day as the "polluted day." Figure 1 shows the red-green-blue (RGB) images of the southern African region on the clean day (the image on the left) and the polluted day (the image on the right). Next, a 60 × 60 km area (latitude = [−15.545 to −14.95]; longitude = [22.85 to 23.45]; blue box in the image on the left and the purple box in the image on the right) centered at Mongu is selected for detailed illustration.

[8] Prior to the calculation of the critical reflectance, the cloud mask algorithm by *Martins et al.* [2002] is applied to MODIS level 1B calibrated reflectance data (0.5 km resolution). After being projected on the grid of 100 pixels per degree (~1 km resolution), the results on both days in the 60 × 60 km range are mapped in Figure 2.

[9] Next, the 3600 (60 × 60) pixels from both images in Figure 2 are evenly divided into a 3 × 3 matrix to produce nine cells with equal numbers of 400 (20 × 20) pixels each. Then, using a scatterplot such as shown in Figure 3 (showing the data from the first cell), we compare the reflectance from pixels in every cell on day 266 to each corresponding pixel on day 250. These data points are then fitted with a robust fit technique (the solid black line in Figure 3; see *DuMouchel and O'Brien* [1989]), which minimizes the effect of potential outlier points. The corresponding reflectance at the TOA that represents the crossing point between the fitted solid black line and the $y = x$ dark dashed black line is by definition the critical reflectance. The intercept of the fitted solid black line on the y axis is defined as the effective path radiance. Our radiative transfer simulations showed that the effective path radiance is ~10 times the AOD difference between the clean day and the polluted day. This result will be used later in section 5 describing the aerosol SSA retrieval.

[10] After we determine the critical reflectance values from MODIS data, the aerosol SSA can be retrieved from a look up table (SSA versus critical reflectance) produced by inputting aerosol models to a Mie code [*Wiscombe*, 1980] and to a radiative transfer model (Santa Barbara DISORT

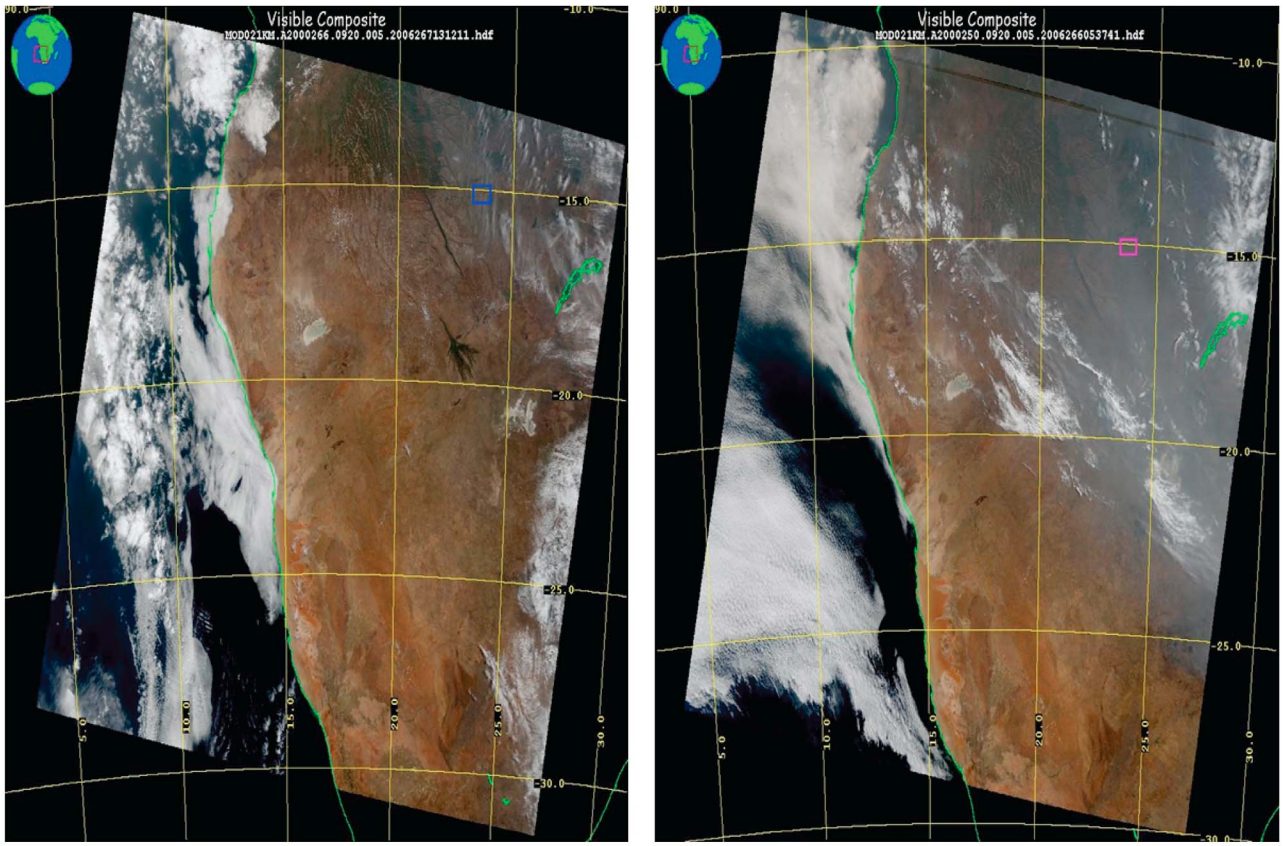

Figure 1. MODIS RGB images over Africa. (left) Julian day 266 of year 2000 (clean day). The blue box represents the 60 × 60 km region around the AERONET site Mongu. (right) Julian day 250 of year 2000 (polluted day). The purple box represents the same 60 × 60 km region as the blue box at left. The blue and purple boxes are used to contrast the clean and polluted days, respectively.

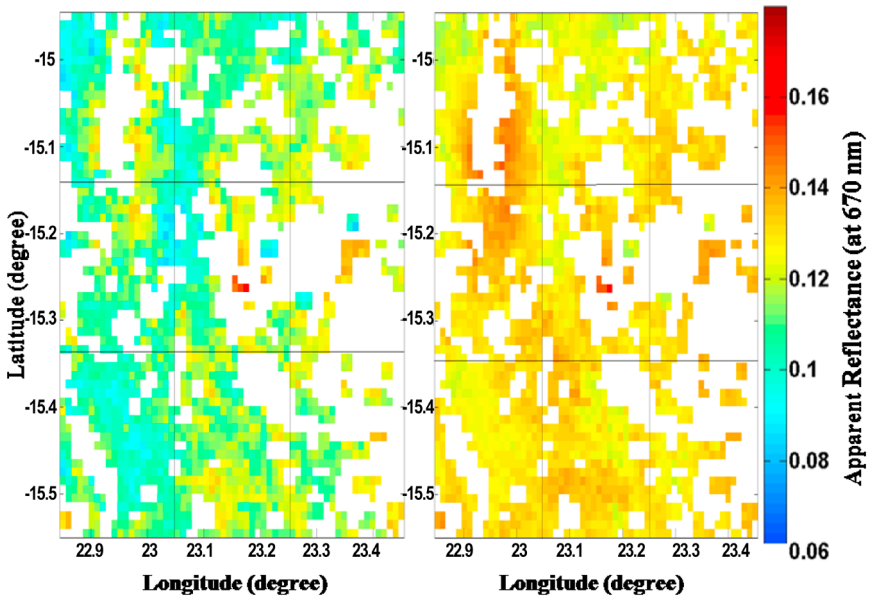

Figure 2. Projected apparent reflectance for the polluted and clean day at 670 nm after applying a common cloud mask to both days. (left) The reflectance in the blue box in Figure 1 with an average AOD (at 670 nm) of 0.36. (right) The reflectance in the purple box in Figure 1 with an average AOD (at 670 nm) of 0.7. The color bar represents the apparent reflectance.

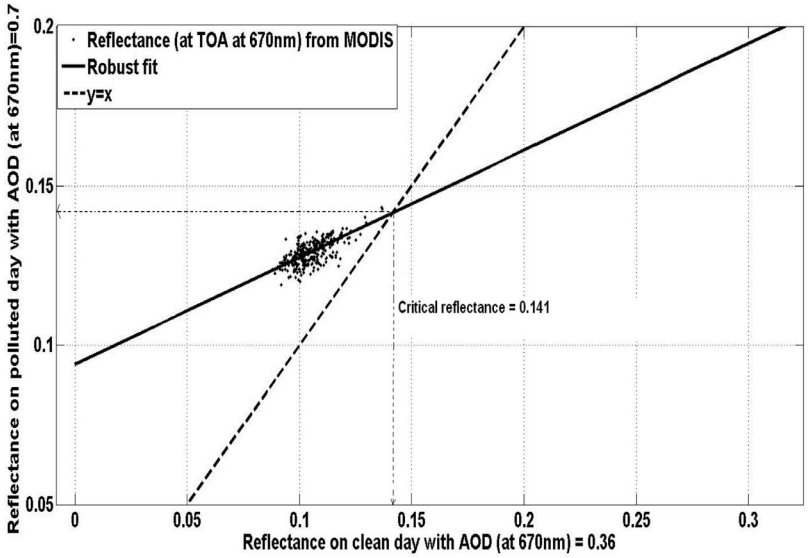

Figure 3. How to calculate critical reflectance using MODIS data from 2 days. The black dots are the scatterplot of the reflectance from the first cell (20 × 20 km range) on the polluted day (the y axis) versus that on the clean day (the x axis). The solid line represents the robust fit of the data. The dark dashed line represents $y = x$, when reflectance (at the top of atmosphere (TOA)) on the clean day equals reflectance (at the TOA) on the polluted day. The reflectance value at the crossing point (as shown by the arrows) between the solid line and the dark dashed line is defined as "critical reflectance." The intercept of the fitted solid line on the y axis is defined as "effective path radiance."

Atmospheric Radiative Transfer (SBDART) by *Ricchiazzi et al.* [1998]). Specifically, aerosol models by *Dubovik et al.* [2002] are used as input parameters, including aerosol size distribution and the real part of refractive index. These simulations will produce a series of phase functions and aerosol SSAs. Next, the following parameters are used to input for SBDART to simulate the reflectance at the top of the atmosphere and then calculate critical reflectance: phase function, SSA, satellite and solar geometry (including solar zenith angle, solar azimuth angle, detector zenith angle, and detector azimuth angle), and MODIS aerosol optical depth (in the clean day and polluted day). By performing these simulations with different SSA and phase functions, we generate a table of SSA versus the critical reflectance parameter. We then use the measured critical reflectance from MODIS (as shown in Figure 3) and this table to retrieve aerosol SSA.

[11] To better understand this application and assess the quality of the aerosol SSA retrieval results, we developed a series of sensitivity tests and validated the results with collocated AERONET measurements. In sections 3, 4, and 5 we show these tests and validation outcomes, discuss factors affecting the retrieval results, and display SSA and AAOD maps.

3. Sensitivity Studies

[12] Aerosol SSA can be retrieved through its unique correlation with the measured critical reflectance. This technique has the distinct advantages of possible global coverage over land, daily measurements, and the no need to know the Earth surface reflectance. It also carries the following potential limitations because of the assumptions used in the simulation: (1) it requires reasonable knowledge of the involved aerosol models, (2) the critical reflectance should be AOD-independent, (3) background aerosols on the clean day and aerosols on the polluted day should have the similar SSA, (4) the Earth surface must exhibit Lambertian reflectance, and (5) there needs to be a large enough AOD difference between these two days. There are other limitations as well, such as the studied area should have enough surface reflectance variability, aerosols should be homogeneously distributed within the studied cell range, and the surface reflectance should be the same on the clean day and the polluted day. In order to understand the importance of these limitations, a series of sensitivity studies have been completed as shown in sections 3.1–3.5.

[13] In addition, to study these sensitivities and validate aerosol SSA retrieved from MODIS, we have to use other available column aerosol SSA measurements. Furthermore, high accuracy of aerosol SSA (e.g., SSA uncertainty of 0.01) is required to make accurate climatic predications. However, the availability of aerosol SSA measurements qualifying these two conditions is significantly limited. The Glory mission (to be launched in November 2010) by NASA might improve this situation in the future. At present, we use AERONET measurements, in which aerosol SSA uncertainty is 0.03 when AOD (at 440 nm) is greater than 0.4 [*Dubovik et al.*, 2000], for our validation. To be consistent, we compare the uncertainty caused by each corresponding limitation also with 0.03, even though our goal is to measure aerosol SSA with much smaller uncertainty. If the difference is significantly smaller than 0.03, we regard that the limitation has little effect on the retrieved aerosol SSA and the uncertainty is acceptable; in contrast, if the difference is greater than 0.03, it indicates that the limitation

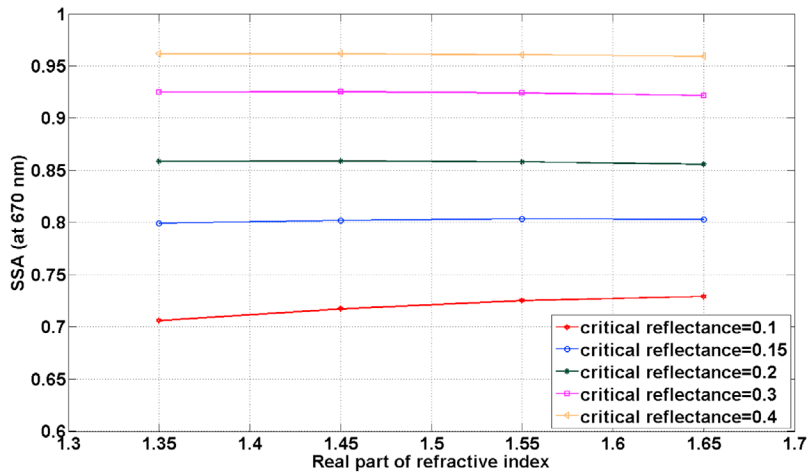

Figure 4. Sensitivity study for the variation of the real part of aerosol refractive index. The x axis represents the real part of the refractive index, and the y axis represents aerosol SSA retrieved for a given critical reflectance. The result shows that the greatest uncertainty of SSA is 0.02 (when critical reflectance equals 0.1 and real refractive index varies from 1.35 to 1.65). Therefore the critical reflectance retrieval of SSA is nearly independent of the real refractive index. The simulation uses the following conditions: AOD (at 670 nm on the clean day) = 0.2; AOD (at 670 nm on clean day) = 0.7; solar zenith angle (SZA) = 26.8°; solar azimuth angle (SAZA) = 37.77°; detector zenith angle (DZA) = 38.65°; and user azimuth angle (phi) = 277.38°.

significantly affects the aerosol SSA retrieval and needs to be considered in the retrieval algorithm.

3.1. Aerosol Models

[14] Aerosol models including aerosol size distribution and the real part of aerosol refractive index from the research by *Dubovik et al.* [2002] are used here as a first guess in our SSA retrieval. These aerosol models are generated from AERONET data before 2000; however, MODIS provides data after 2000. To see whether the models can represent the data from the years after 2000, the real part of aerosol refractive index is studied, and the result shows that the mean real part of the refractive index for biomass burning aerosols over Mongu is 1.51, which agrees well with the value of 1.51 from *Dubovik et al.*'s [2002, Table 1] model. Similar comparisons over other AERONET sites also show good agreements between the data before and after 2000. Therefore, Dubovik et al.'s aerosol models are used in our research to represent the aerosol properties.

[15] In addition, the result of our sensitivity studies presented in Figure 4 show that the SSA retrieval with the critical reflectance technique is nearly independent of the real part of refractive index assumption from the pre-established aerosol model. In the worst case, as shown in Figure 4, for real refractive index variation from 1.35 to 1.65, the retrieved SSA varies by a maximum of 0.02 (when critical reflectance equals 0.1), which is an acceptable uncertainty compared to AERONET 0.03 error. This analysis indicates that the sensitivity to real refractive index is relatively small and a relatively coarse first guess is acceptable.

[16] Furthermore, the sensitivity study of aerosol SSA with the variability of biomass burning aerosol size distribution also shows acceptable uncertainty. In aerosol models by *Dubovik et al.* [2002], bimodal volume size distribution is a function of AOD. Specifically, for forest biomass burning aerosols, when AOD (at 0.47 μm) varies from 0.4 to 2, the median radius varies from 0.15 μm to 0.21 μm for the fine mode and from 3.50 μm to 4.43 μm for the coarse mode. For critical reflectance varying from 0.2 to 0.55, the maximum uncertainty of SSA is 0.02 (when critical reflectance equals 0.2 and aerosol size distribution has the maximum variation: the median radius varies from 0.15 to 0.21 μm for the fine mode and from 3.50 μm to 4.43 μm for the coarse mode). Therefore, the sensitivity of MODIS aerosol SSA retrieval to smoke aerosol size distribution is acceptable. This paper focus on applying the critical reflectance retrieval to biomass burning aerosols, which may also be applicable to pollution and other fine mode dominated aerosols. The situation will be different and more complicated if we retrieve SSA of mixed aerosol types, for example mixture of dust and smoke.

3.2. Dependence of Critical Reflectance on AOD

[17] The definition of critical reflectance assumes it to be AOD-independent [*Fraser and Kaufman*, 1985, Figure 2]. Nevertheless, a closer look at the crossing point shows that the simulated lines cross each other in the neighborhood of one point, instead of exactly at that point [*Kaufman*, 1987], which implies that critical reflectance is weakly dependent on AOD. A sensitivity study to determine the importance of this effect was performed. According to Figure 5, when AOD on the polluted day increases from 0.5 to 1.0 and AOD on the clean day remains as 0.1, the variation of the critical reflectance is 0.01. This extreme case with the uncertainty of AOD between 0.5 to 1.0 leads to an SSA uncertainty of ± 0.0125 (at SSA = 0.8) and ± 0.005 (at SSA = 0.95), as in Figure 6, which are both significantly smaller than the 0.03 uncertainty from AERONET. In reality, we will have a much better handle on the AOD uncertainties and will significantly reduce these error bars.

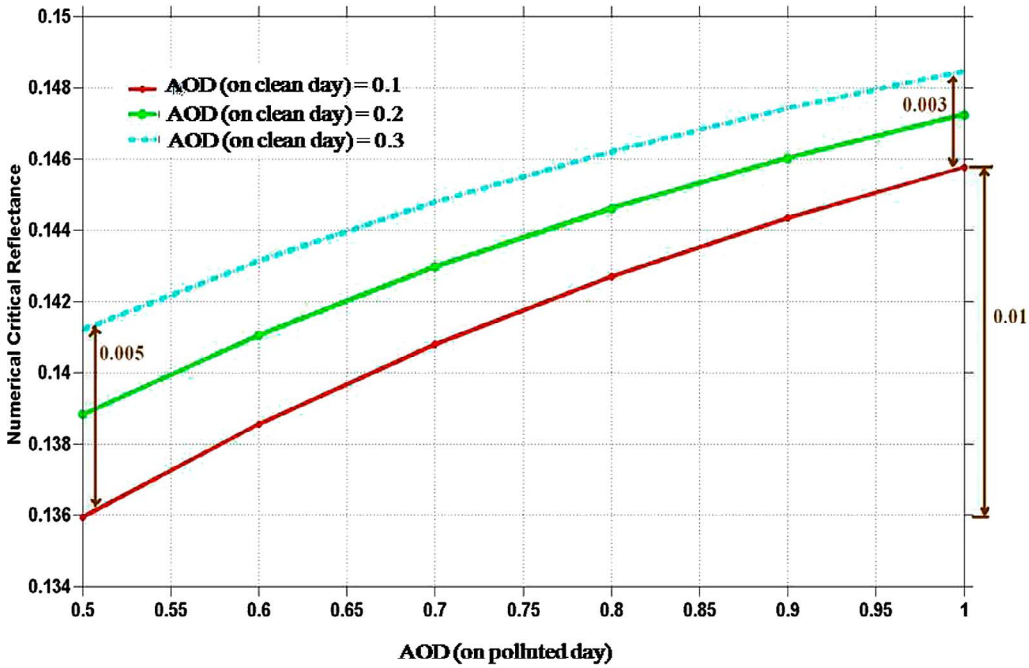

Figure 5. AOD dependence of the critical reflectance. The x axis represents AOD (at 670 nm) on a polluted day, and the y axis represents the calculated critical reflectance for AOD values (at 670 nm on a clean day) of 0.1, 0.2, and 0.3. The simulations use the following conditions: solar zenith angle (SZA) = 26.8°; solar azimuth angle (SAZA) = 37.77°; detector zenith angle (DZA) = 38.65°; user azimuth angle (phi) = 277.38°; wavelength = 0.67 μm; and SSA = 0.8. When AOD on the clean day varies from 0.1 to 0.3, the variation of critical reflectance is 0.005 (AOD of 0.5 on the polluted day) and 0.003 (AOD of 1 on the polluted day). In addition, when AOD on the polluted day varies from 0.5 to 1, the variation of critical reflectance is 0.01(AOD of 0.1 on the clean day).

3.3. Varying SSA of Aerosols on the Clean Versus Polluted Days

[18] The basic critical reflectance technique also assumes that aerosols in both clean and polluted days have the same SSA. However, this condition might not be satisfied in all cases. To study how aerosol SSA variation between both days affects the retrieval results, we assume that on the polluted day aerosol SSA (at 0.67 μm) is 0.898 and AOD is

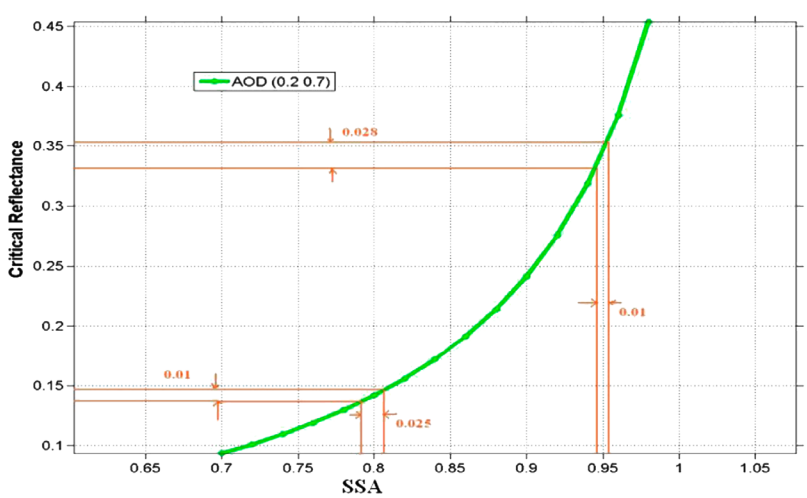

Figure 6. Sensitivity study of aerosol SSA (at 670 nm) to varying critical reflectance. The x axis represents SSA, and the y axis represents critical reflectance. The solid curve shows the unique correlation between critical reflectance and SSA. AOD on the clean (polluted) day is 0.2 (0.7). It shows that the critical reflectance uncertainty of 0.01 leads to an SSA uncertainty of 0.025 (when SSA = 0.8). Similarly, a critical reflectance uncertainty of 0.028 causes an SSA total uncertainty of 0.01 (when SSA = 0.95).

Table 1. Sensitivity Study for Varying Aerosol SSA Between the Clean Day and the Polluted Day[a]

Clean-Day SSA	Critical Reflectance	Retrieved SSA	Retrieved SSA Minus Polluted-Day SSA
	Polluted-Day SSA = 0.898		
0.986	0.205	0.872	−0.026
0.934	0.226	0.887	−0.011
0.855	0.263	0.909	0.011
0.824	0.281	0.917	0.019
	Polluted-Day SSA = 0.972		
0.993	0.461	0.966	−0.006
0.986	0.473	0.968	−0.004
0.934	0.601	0.983	0.011
0.910	0.691	0.990	0.018

[a]Wavelength = 0.67 μm; aerosol optical depth on the clean day = 0.2; AOD on the polluted day = 0.7; solar zenith angle = 26.8°; solar azimuth angle = 37.77°; detector zenith angle = 38.65°; detector azimuth angle = 277.38°. Real part of the refractive index = 1.51. Results show that the uncertainty caused by varying aerosol SSA between the clean day and the polluted day is acceptable.

0.7, on the clean day AOD is 0.2 and SSA varies from 0.986 to 0.824 as in Table 1. The results of a similar analysis of SSA are also shown in Table 1: on the polluted day SSA is 0.972 and varies from 0.910 to 0.993 on the clean day. The real part refractive index is kept at 1.51 for both days. The results in Table 1 show that the difference between the retrieved SSA and the SSA on the polluted day varies between −0.026 to 0.019 (when SSA on the polluted day is 0.898) and −0.006 to 0.018 (when SSA on the polluted day is 0.972). Considering these differences are still smaller than the AERONET aerosol SSA uncertainty 0.03 even under extreme cases, we regard that varying the aerosol SSA between the clean day and the polluted day affects retrieved aerosol SSA with acceptable uncertainty.

3.4. Detector Zenith Angle

[19] The data analysis shows that detector zenith angle (DZA) affects retrieval results when it is bigger than 40°. This issue can be demonstrated through the results of a group of cases over Senanga in 2000. According to Figure 7, when DZA is greater than 40°, the deviation of MODIS SSA from AERONET SSA increases as DZA increases. In addition, in order to keep the deviation below 0.03, DZA needs to be smaller than 40°. This result is likely because our retrieval applies the simplified assumption of Lambertian Earth surface reflectance, instead of the reflectance with angular distribution usually modeled by the bidirectional reflectance distribution function (BRDF) [*Maignan et al.*, 2004]. This issue will be addressed in more detail in our future research with the incorporation of the Earth surface BRDF in radiative transfer simulations. At this point, we will only select cases with DZA < 40° as a quality assurance procedure. The similar analysis of SSA with scattering angle and SSA with solar zenith angle does not show SSA dependence on these two geometries as its dependence on DZA.

3.5. AOD Difference Between the Clean Day and the Polluted Day

[20] Besides DZA, AOD difference (between the clean day and the polluted day) affects the signal-to-noise ratio and hence the accuracy of the SSA retrieval. A group of cases over Mongu in 2000 is used to study this issue. As

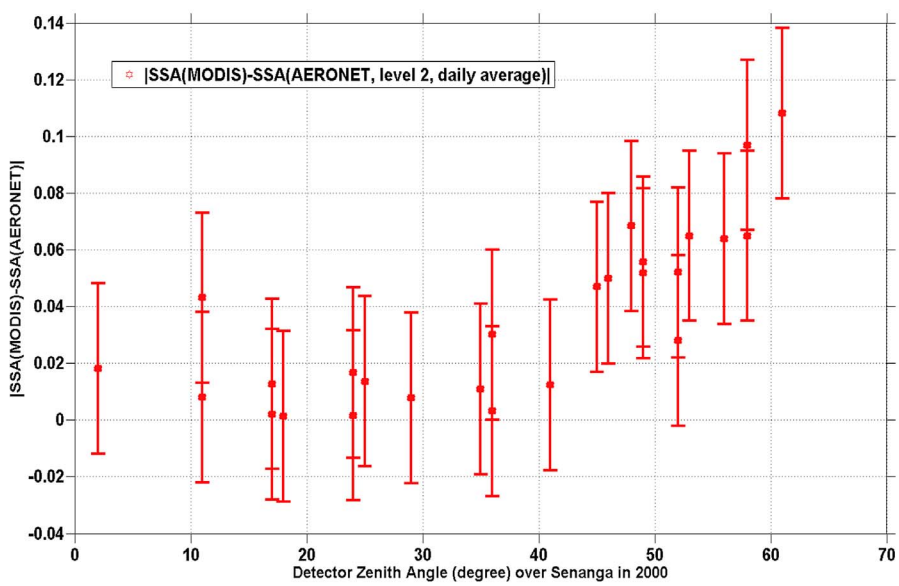

Figure 7. Detector zenith angle (DZA) affects aerosol SSA retrievals. The *x* axis represents DZA for each case, and the *y* axis represents the absolute difference between the retrieved aerosol SSA (over Senanga in 2000) from MODIS on Terra and AERONET level 2 daily averaged aerosol SSA. The bar over each data point represents the AERONET SSA uncertainty of 0.03. The result indicates that the difference between aerosol SSA retrieved from MODIS and from AERONET increases as DZA increases. This effect is likely caused by the simplified assumption of a Lambertian surface reflectance in the radiative transfer simulations.

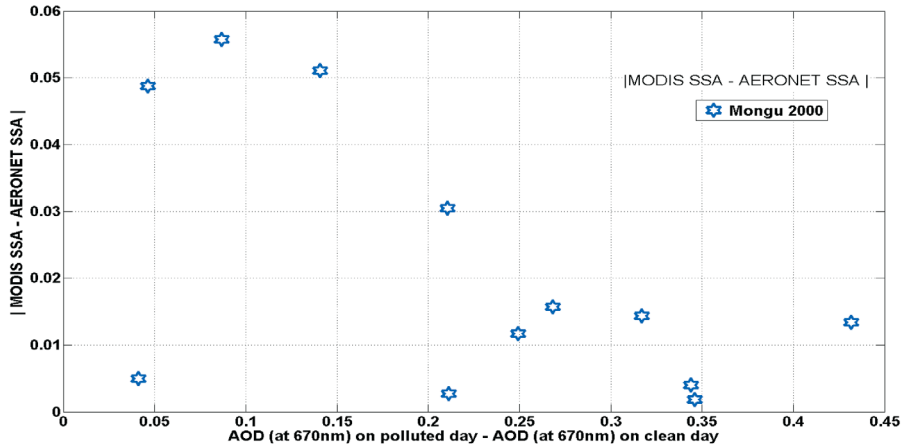

Figure 8. AOD differences affect aerosol SSA retrievals. The *x* axis represents the AOD difference at 670 nm between the clean day and the polluted day, and the *y* axis represents the absolute difference between aerosol SSA (over Mongu in 2000) retrieved from MODIS and AERONET level 2 daily averaged aerosol SSA. The result shows that AOD difference needs to be greater than 0.2 in order to produce a high enough signal-to-noise ratio and to keep the deviation of MOIDS SSA from AERONET SSA below 0.03.

shown in Figure 8, in order to keep the deviation of MODIS SSA from AERONET SSA below 0.03, the AOD difference needs to be greater than 0.2 to have a high enough signal-to-noise ratio. In a similar manner, we did another two studies: (1) the difference between MODIS SSA and AERONET SSA versus AERONET SSA and (2) the difference between MODIS SSA and AERONET SSA versus AOD on the polluted day. The results do not show any obvious correlations between these parameters.

[21] In summary, these sensitivity studies concerning the aerosol model about the real part of aerosol refractive index, AOD dependence of the critical reflectance, and variations of the aerosol SSA between on the clean day and the polluted day show that the uncertainties of retrieved aerosol SSA caused by these factors are acceptable for a satellite retrieval of aerosol SSA. In addition, to produce retrieval results in good agreement with AERONET measurements, a case need to satisfy two conditions: DZA is smaller than 40°, and the AOD difference between clean day and polluted day is bigger than 0.2.

4. Algorithm and Validation Strategy

[22] After doing sensitivity studies, we apply the critical reflectance technique on some cases of MODIS data to retrieve aerosol SSA. Our studied regions are dominated by biomass burning aerosols and are collocated with the AERONET sites as follows: Senanga (African savanna), Mongu (African savanna), Mwinilunga (African savanna), and Alta Floresta (Amazon forest). The studied cases are selected on the basis of evaluating MODIS RGB images, MODIS data, and AERONET data to determine that: (1) cloud cover is minimal over the study areas on both the clean day and polluted day, 16 days apart; (2) MODIS DZA is less than 40°; (3) these two days have AOD difference (at 670 nm) greater than or equal to 0.2; and (4) AERONET has level 2 aerosol SSA retrievals available for the polluted day. All retrieval results are validated with collocated AERONET retrieval products, and regional SSA and AAOD maps were produced and will be shown in section 5.

[23] As discussed in section 1, aerosol SSA can be retrieved from the critical reflectance measurements performed with MODIS data as shown in Figures 1–3. Next, as quality control, we have removed cells bearing any of the following properties: (1) having negative critical reflectance; (2) SSA greater than 1 or smaller than 0; (3) an SSA uncertainty derived from robust fitting [*DuMouchel and O'Brien*, 1989] greater than 0.03; (4) root mean square error (RMSE) greater than 0.006 between the data points and the fitting results; and (5) the effective path radiance smaller than 0.02 (corresponding to an AOD difference greater than 0.2.

[24] In addition, recent studies have shown that aerosol SSA varies with biomass burning stages and the aerosol aging process [*Abel et al.*, 2003; *Zaveri et al.*, 2010]. Therefore, AERONET level 2 aerosol SSA measured at the closest time to the MODIS overpass time is used for the validation, instead of the daily average. In these AERONET level 2 closest time SSA retrievals, the SZA is in the range of 53 to 76°. We compare the AERONET SSA with the mean and the standard deviation of our retrieved aerosol SSA. In order to calculate aerosol SSA variance with less than nine samples, we apply a chi square distribution correction and set a confidence interval of 50% [*Bevington*, 1969].

[25] According to our quality assurance analysis, accurate biomass burning aerosol SSA can be retrieved with the critical reflectance technique at 0.47, 0.55, and 0.67 μm channels; however, there is not enough signal-to-noise ratio at the other four aerosol channels (0.86, 1.24, 1.64, and 2.12 μm) to retrieve biomass burning aerosol SSA; that is, there are no cells left out of nine total after applying our data quality criteria. Next, we validate aerosol SSA retrieved from MODIS data with collocated AERONET measure-

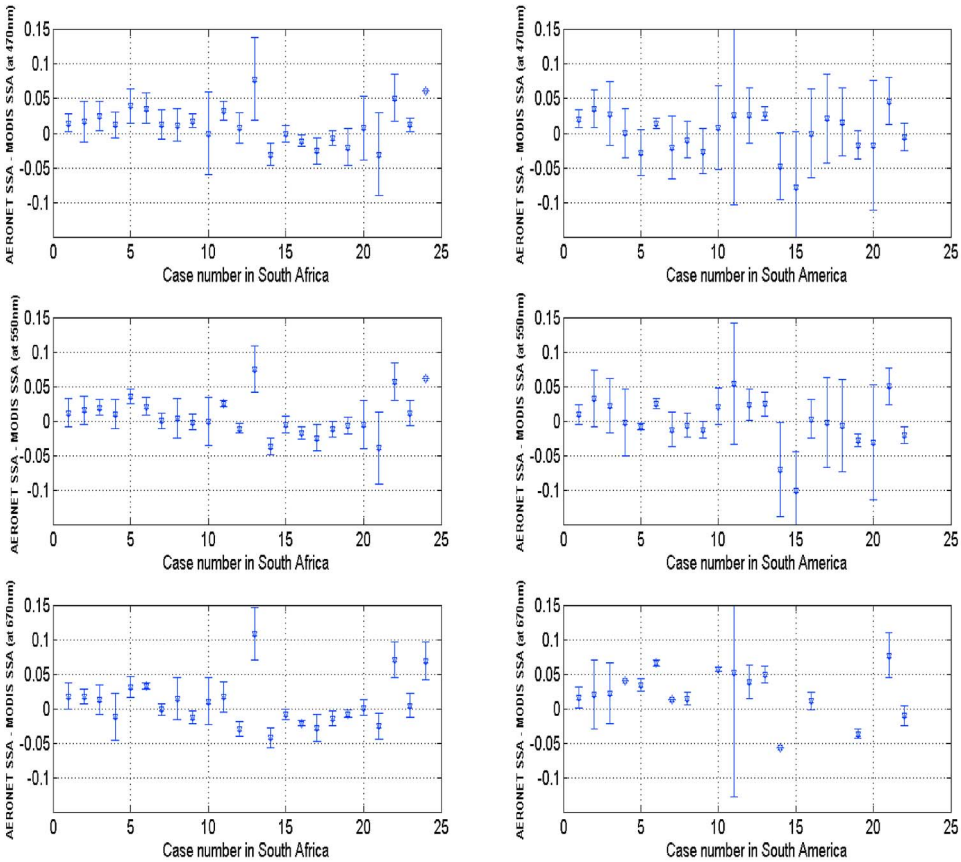

Figure 9. Comparison of aerosol SSA retrieved from MODIS with collocated AERONET measurement in (left) South Africa and (right) South America. The *x* axis represents the case numbers, and the *y* axis represents the difference between aerosol SSA from AERONET and from MODIS. In addition, bars over each data point represent SSA variance (among the remaining cells in 60 × 60 km range) at a 50% of confidence interval and with a chi square distribution correction. Since AERONET SSA has an uncertainty of 0.03, the aerosol SSA retrieved from MODIS agrees well with AERONET measurements (68% by only considering the mean; 88% by considering the mean and the variance); that is, the absolute difference between aerosol SSA from AERONET and MODIS is smaller than 0.03. The result also shows that aerosol SSA has a larger spatial variation in South America than in South Africa.

ments (AERONET SSAs at 0.47 and 0.55 μm used here is the first-order interpolation AERONET SSAs at 0.440 and 0.676 μm).

5. Results

5.1. Retrieving and Validating Aerosol SSA Over a 60 × 60 km Area

[26] Aerosol SSA was retrieved by applying the algorithm described above, and the result was compared with collocated AERONET measurements in South Africa and South America. According to Figure 9, ~68% (by only considering the mean value) and 88% (by considering the mean value and the variance) of all the studied cases satisfies the requirement that the absolute difference between MODIS SSA and AERONET SSA is smaller than 0.03. Figure 9 also indicates that aerosol SSA has a larger spatial variation (represented by larger error bars) in South America than in South Africa. Specifically, the mean value of the sample variance is 0.04 for the cases in South America and 0.02 in South Africa.

[27] In addition, the comparison of the mean and sample variance of aerosol SSA over time for each studied locations between MODIS retrievals and AERONET measurements is displayed in Table 2. According to Table 2, aerosol SSA retrievals from MODIS are biased lower than AERONET measurements over Mwinilunga, which might be caused by problems in either MODIS or AERONET retrievals. Table 2 also shows that climatologically for the other sites, MODIS retrieval results agree well with AERONET measurements. The biggest difference between MODIS mean and AERONET mean is 0.02. This indicates that aerosol SSA retrieved from MODIS is accurate enough to be used in climatologic studies.

5.2. Regional Aerosol SSA and AAOD Maps

[28] The above validation results show that applying the critical reflectance technique with MODIS data can retrieve aerosol SSA in reasonable agreement with AERONET

Table 2. Mean and Sample Variance of Aerosol SSA From MODIS Retrievals and AERONET Measurements Over Different Locations[a]

AERONET Site	SSA at 470 nm		SSA at 550 nm		SSA at 670 nm	
	AERONET	MODIS	AERONET	MODIS	AERONET	MODIS
Alta Floresta	0.92 ± 0.02 (22 cases)	0.92 ± 0.03	0.91 ± 0.03 (22 cases)	0.92 ± 0.03	0.92 ± 0.03 (18 cases)	0.90 ± 0.03
Senanga	0.86 ± 0.01 (7 cases)	0.87 ± 0.01	0.85 ± 0.01 (7 cases)	0.87 ± 0.01	0.84 ± 0.01 (7 cases)	0.86 ± 0.01
Mongu	0.88 ± 0.02 (14 cases)	0.86 ± 0.02	0.87 ± 0.03 (14 cases)	0.86 ± 0.02	0.86 ± 0.03 (14 cases)	0.84 ± 0.02
Mwinilunga	0.90 ± 0.02 (3 cases)	0.86 ± 0.01	0.90 ± 0.02 (3 cases)	0.85 ± 0.01	0.89 ± 0.03 (3 cases)	0.84 ± 0.01

[a]MODIS retrievals are biased smaller than AERONET measurements over Mwinilunga, which might be caused by problems in either MODIS or AERONET retrievals. Over other sites the maximum difference between MODIS SSA and AERONET SSA is 0.02. These high-accuracy aerosol SSA retrievals from MODIS indicate its promising application in climatological studies over a given region.

results within AERONET uncertainty levels. Next, by expanding the studied areas, we produce regional aerosol SSA and AAOD maps, which have wide applications in climate modeling and radiative forcing calculations. For example, Figures 10–13 show aerosol SSA and AAOD (at 470 nm) maps over South Africa and South America. In addition, the means and the standard deviations (representing the spatial variation) of aerosol SSA at 470, 550, and 670 nm, as well as the AAOD at these three channels over both regions are listed in Table 3. Again, these results also indicate that aerosol SSA has a larger spatial variation in South America than in South Africa, which is in consistent with the results from Figure 9. In addition, AAOD data also shows that it has bigger (or similar) spatial variation in South America than in South Africa. The SSA map over the Amazon shows significant connection between the distribution of SSA and AOD. All results (AOD, SSA, and AAOD) show greater values in the northern part of the Amazon, which is compatible with the particle properties and aerosol loading of forest smoke versus Cerrado smoke [*Dubovik et al.*, 2002].

6. Conclusions

[29] In this research, the critical reflectance technique is applied on MODIS data from biomass burning regions by

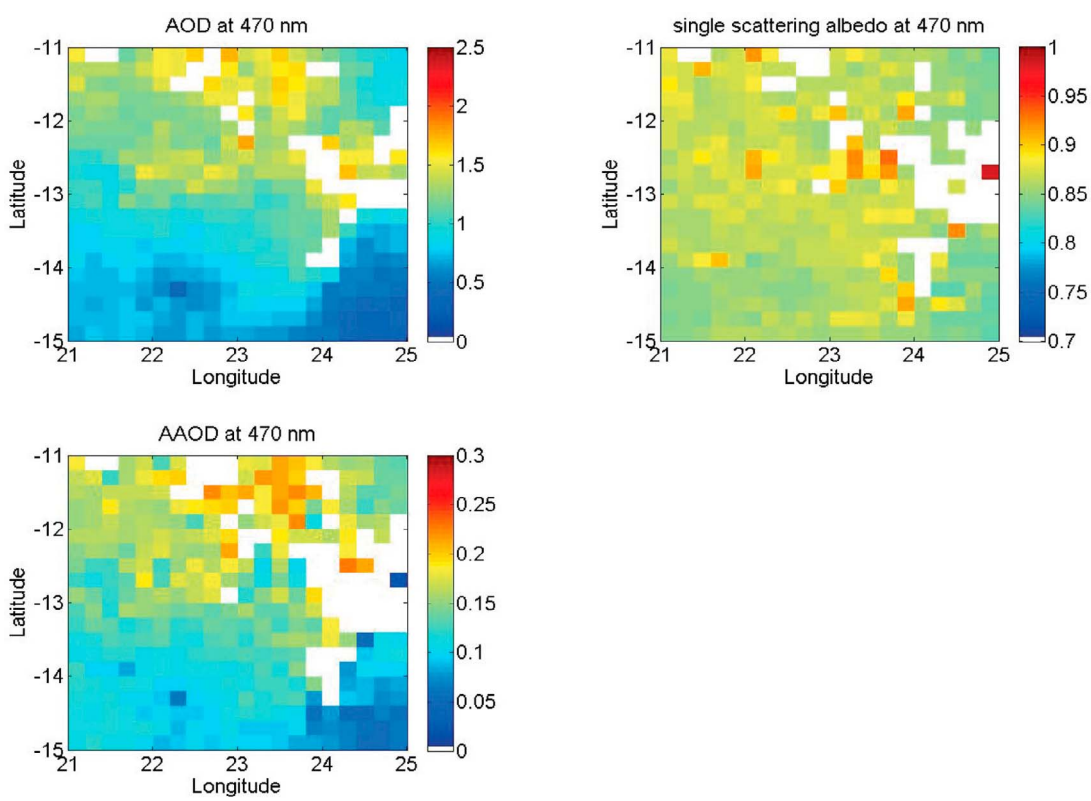

Figure 10. Maps of regional AOD, aerosol SSA, and AAOD (at 470 nm) over South Africa with latitude = [−15 to −11] and longitude = [21 to 25] on day 254 in 2000 (with day 238 as the clean day). All images have a resolution of 20 × 20 km.

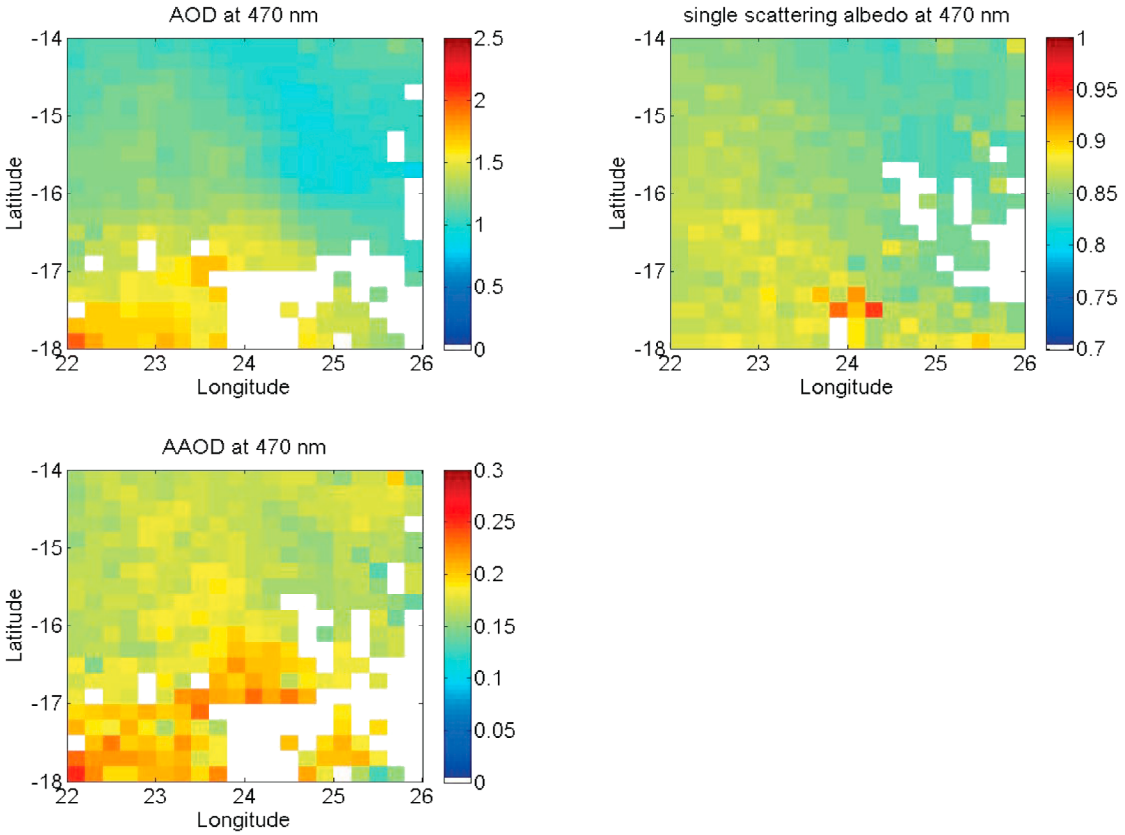

Figure 11. Maps of regional AOD, aerosol SSA, and AAOD (at 470 nm) over South Africa with latitude = [−18 to −14] and longitude = [22 to 26] on day 250 in 2000 (with day 266 as the clean day). All images have a resolution of 20 × 20 km.

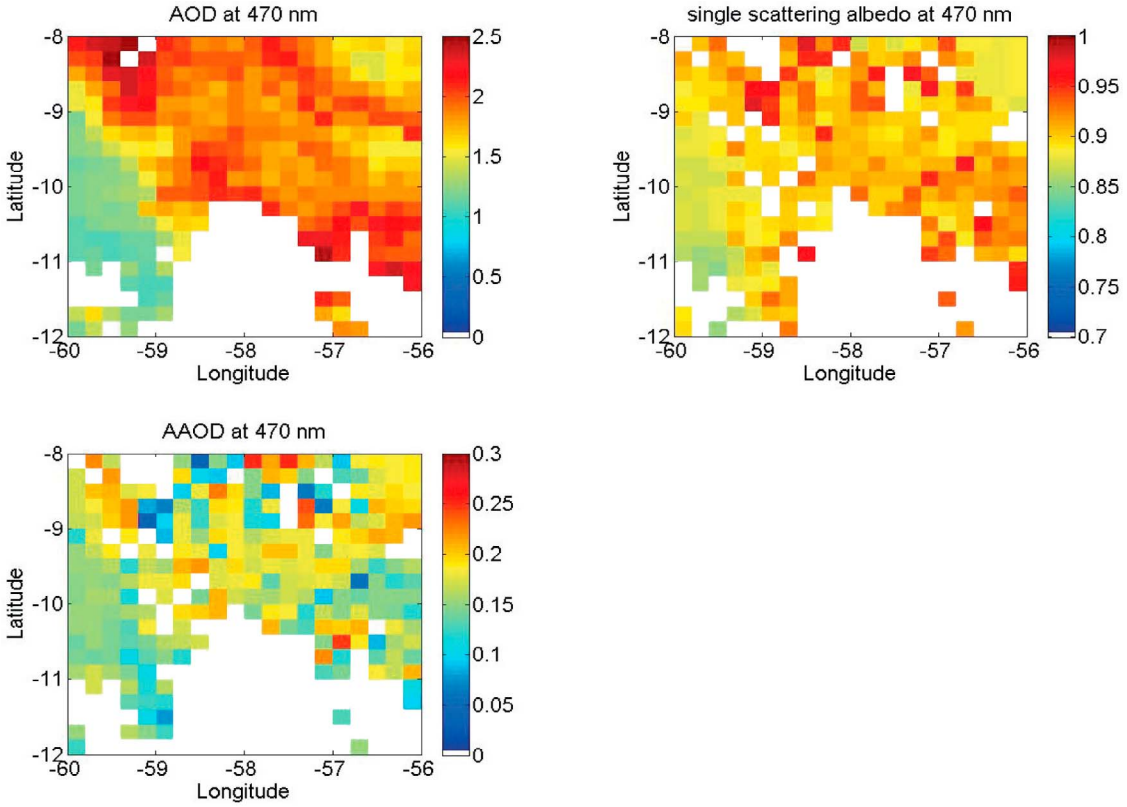

Figure 12. Maps of regional AOD, aerosol SSA, and AAOD (at 470 nm) over South America with latitude = [−12 to −8] and longitude = [−60 to −56] on day 241 in 2006 (with day 225 as the clean day). All images have a resolution of 20 × 20 km.

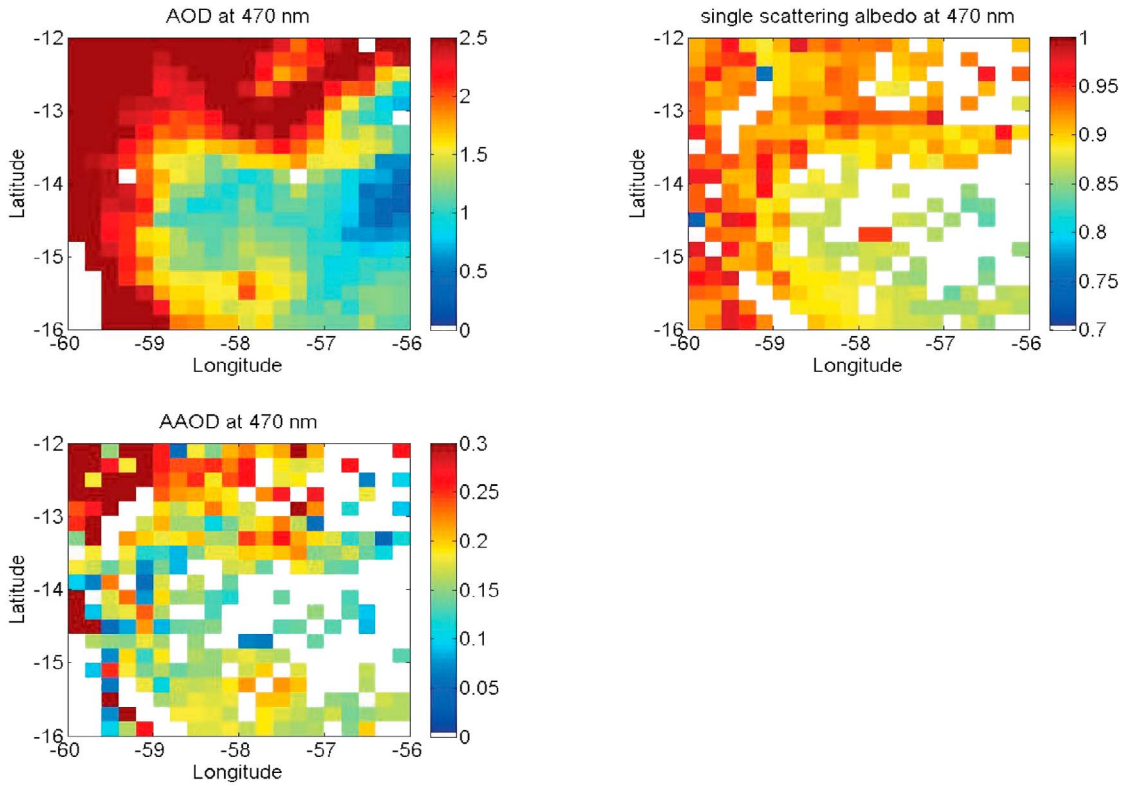

Figure 13. Maps of regional AOD, aerosol SSA, and AAOD (at 470 nm) over South America with latitude = [−16 to −12] and longitude = [−60 to −56] on day 252 in 2004 (with day 268 as the clean day). All images have a resolution of 20 × 20 km.

comparing reflectance at TOA in two days (a clean day and a polluted day 16 days apart) to retrieve the aerosol SSA on the polluted day. First, this study describes a method to determine critical reflectance from MODIS data. Second, sensitivity studies that examine a range of aerosol conditions expected for our study areas (including aerosol models, the variation of the real part of aerosol refractive index, dependence on biomass burning aerosol size distribution from aerosol models by *Dubovik et al.* [2002], AOD dependence of the critical reflectance, and the variation of aerosol SSA between a clean day and a polluted day) indicate that these factors have manageable effect on the retrieval results. In the mean time, a DZA smaller than 40° and an AOD difference greater than 0.2 are required to

Table 3. Mean and Standard Deviation of AAOD and Aerosol SSA for the Same Cases as Shown in Figures 10–13[a]

Case Information	AAOD: Mean ± SD			Aerosol SSA: Mean ± SD		
	470 nm	550 nm	670 nm	470 nm	550 nm	670 nm
Latitude = [−15 to −11]; longitude = [21 to 25] over South Africa; on day 254 in 2000	0.13 ± 0.04	0.11 ± 0.04	0.10 ± 0.03	0.86 ± 0.02	0.84 ± 0.02	0.82 ± 0.02
Latitude = [−18 to −14]; longitude = [22 to 26] over South Africa; on day 250 in 2000	0.18 ± 0.02	0.15 ± 0.02	0.14 ± 0.02	0.86 ± 0.02	0.84 ± 0.02	0.81 ± 0.02
Latitude = [−12 to −8]; longitude = [−60 to −56] over South America; on day 241 in 2006	0.16 ± 0.04	0.13 ± 0.04	0.14 ± 0.04	0.90 ± 0.03	0.90 ± 0.03	0.87 ± 0.04
Latitude = [−16 to −12]; longitude = [−60 to −56] over South America; on day 252 in 2004	0.20 ± 0.12	0.14 ± 0.05	0.14 ± 0.06	0.91 ± 0.04	0.92 ± 0.03	0.91 ± 0.03

[a]Data show that aerosol SSA has a larger spatial variation in South America than in South Africa, which is consistent with the result from Figure 9. Figures 10–13 also show that AAOD has bigger (or similar) spatial variation in South America than in South Africa. SD, standard deviation.

provide accurate retrieved aerosol SSA values. We did not test the effect of particle shape on retrievals of SSA because the smoke aerosol is expected to be mostly spherical. Critical reflectance retrievals and subsequent mapping to SSA may show greater sensitivities and uncertainties for other aerosol types and different surfaces. Aerosol mixtures of smoke and dust may be especially difficult. These factors might affect the general applicability of the critical reflectance technique to retrieve accurate aerosol absorption properties globally with generic aerosol conditions.

[30] Validation results show that the retrieved aerosol SSA from MODIS agrees well with collocated AERONET measurements. The ensemble average SSA results from the critical reflectance techniques are in good agreement with collocated AERONET ensemble averages, within 0.02 in all cases, except for the Mwinilunga station that seems to present some artificial bias. Moreover, the analysis of aerosol SSA from MODIS retrievals concludes that aerosol SSA has a larger spatial variation in South America than in South Africa, and that we can see the South American north–south gradient in SSA and AOD reported by previous studies. Likewise the critical reflectance method also reproduces findings that show African savanna SSA about 0.08 to 0.09 lower than what is measured in the Amazon forest.

[31] However, the power of the critical reflectance method is not in its ability to reproduce previous point measurements or retrievals, either spatially (AERONET) or temporally (field experiments). The true contribution of the critical reflectance method, demonstrated here, is to offer frequent quantitative measures of spectral aerosol SSA over broad regions, and to capture the spatial and temporal variability of this essential particle property.

[32] **Acknowledgments.** We would like to thank NASA for funding this project under grant NNX08AJ78G. We also would like to thank the MODIS and AERONET teams for their excellent work on the instrument development, maintenance, and calibration. We thank their effort on data quality control and for providing data to the public, as well. Thanks also go to Kelley Wells, Alexandre Correia, Tom Eck, Tianle Yuan, Ralph Kahn, and the anonymous reviewers for their constructive comments and suggestions.

References

Abel, S. J., J. M. Haywood, E. J. Highwood, J. Li, and P. R. Buseck (2003), Evolution of biomass-burning aerosol properties from an agricultural fire in southern Africa, *Geophys. Res. Lett.*, *30*(15), 1783, doi:10.1029/2003GL017342.

Ackerman, T. P., and O. B. Toon (1981), Absorption of visible radiation in atmosphere containing mixtures of absorbing and nonabsorbing particles, *Appl. Opt.*, *20*, 3661–3668, doi:10.1364/AO.20.003661.

Ackerman, A. S., O. B. Toon, D. E. Stevens, A. J. Heymsfield, V. Ramanathan, and E. J. Welton (2000), Reduction of tropical cloudiness by soot, *Science*, *288*, 1042–1047, doi:10.1126/science.288.5468.1042.

Atwater, M. A. (1970), Planetary albedo changes due to aerosols, *Science*, *170*, 64–66, doi:10.1126/science.170.3953.64.

Bevington, P. R. (1969), *Data Reduction and Error Analysis for the Physical Sciences*, McGraw-Hill, New York.

Bond, T. C., T. L. Anderson, and D. Campbell (1999), Calibration and inter comparison of filter-based measurements of visible light absorption by aerosols, *Aerosol Sci. Technol.*, *30*, 582–600, doi:10.1080/027868299304435.

Clarke, A. D., K. J. Noone, J. Heintzenberg, S. G. Warren, and D. S. Covert (1967), Aerosol light absorption measurement techniques: Analysis and intercomparisons, *Atmos. Environ.*, *21*, 1455–1465, doi:10.1016/0004-6981(67)90093-5.

Davidi, A., I. Koren, and L. Remer (2009), Direct measurements of the effect of biomass burning over the Amazon on the atmospheric temperature profile, *Atmos. Chem. Phys. Discuss.*, *9*, 12,007–12,025.

Dubovik, O., B. N. Holben, Y. J. Kaufman, M. Yamasoe, A. Smirnov, D. Tanré, and I. Slutsker (1998), Single-scattering albedo of smoke retrieved from the sky radiance and solar transmittance measured from ground, *J. Geophys. Res.*, *103*, 31,903–31,923, doi:10.1029/98JD02276.

Dubovik, O., et al. (2000), Accuracy assessments of aerosol optical properties retrieved from AERONET Sun and sky-radiance measurements, *J. Geophys. Res.*, *105*, 9791–9806, doi:10.1029/2000JD900040.

Dubovik, O., B. N. Holben, T. F. Eck, A. Smirnov, Y. J. Kaufman, M. D. King, D. Tanré, and I. Slutsker (2002), Variability of absorption and optical properties of key aerosol types observed in worldwide locations, *J. Atmos. Sci.*, *59*, 590–608, doi:10.1175/1520-0469(2002)059<0590:VOAAOP>2.0.CO;2.

DuMouchel, W. H., and F. L. O'Brien (1989), Integrating a robust option into a multiple regression computing environment, paper presented at *Computer Science and Statistics: The 21st Symposium on the Interface*, Am. Stat. Assoc., Alexandria, Va.

Feingold, G., H. Jiang, and J. Y. Harrington (2005), On smoke suppression of clouds in Amazonia, *Geophys. Res. Lett.*, *32*, L02804, doi:10.1029/2004GL021369.

Fraser, R. S., and Y. J. Kaufman (1985), The relative importance of aerosol scattering and absorption in remote sensing, *IEEE Trans. Geosci. Remote Sens.*, *23*, 625–633, doi:10.1109/TGRS.1985.289380.

Hansen, A. D. A., H. Rosen, and T. Novakov (1984), The aethalometer—An instrument for the real-time measurement of optical absorption by aerosol particles, *Sci. Total Environ.*, *36*, 191–196, doi:10.1016/0048-9697(84)90265-1.

Hansen, J., M. Sato, R. Ruedy, A. Lacis, and V. Oinas (2000), Global warming in the twenty-first century: An alternative scenario, *Proc. Natl. Acad. Sci. U. S. A.*, *97*, 9875–9880, doi:10.1073/pnas.170278997.

Heintzenberg, J., R. J. Charlson, A. D. Clarke, C. Liousse, V. Ramaswamy, K. P. Shine, M. Wendish, and G. Helas (1997), Measurements and modelling of aerosol single scattering albedo: Progress, problems and prospects, *Beitr. Phys. Atmos.*, *70*, 249–263.

Herman, R. J., K. P. Bhartia, O. Torres, C. Hsu, C. Seftor, and E. Celarier (1997), Global distribution of UV-absorbing aerosols from Nimbus 7/TOMS data, *J. Geophys. Res.*, *102*, 16,911–16,922, doi:10.1029/96JD03680.

Hsu, N. C., J. R. Herman, and C. Weaver (2000), Determination of radiative forcing of Saharan dust using combined TOMS and ERBE data, *J. Geophys. Res.*, *105*(D16), 20,649–20,661, doi:10.1029/2000JD900150.

Hu, R. M., R. V. Martins, and T. D. Fairlie (2007), Global retrieval of columnar aerosol single-scattering albedo from space-based observations, *J. Geophys. Res.*, *112*, D02204, doi:10.1029/2005JD006832.

Hu, R. M., R. S. Sokhi, and B. E. A. Fisher (2009), New algorithms and their application for satellite remote sensing of surface PM2.5 and aerosol absorption, *J. Aerosol Sci.*, *40*, 394–402, doi:10.1016/j.jaerosci.2009.01.005.

Ichoku, C., L. A. Remer, Y. J. Kaufman, R. Levy, D. A. Chu, D. Tanré, and B. N. Holben (2003), MODIS observation of aerosols and estimation of aerosol radiative forcing over southern Africa during SAFARI 2000, *J. Geophys. Res.*, *108*(D13), 8499, doi:10.1029/2002JD002366.

Jeong, M.-J., and N. C. Hsu (2008), Retrievals of aerosol single-scattering albedo and effective aerosol layer height for biomass-burning smoke: Synergy derived from "A-Train" sensors, *Geophys. Res. Lett.*, *35*, L24801, doi:10.1029/2008GL036279.

Kalashnikova, O. V., and R. Kahn (2006), Ability of multiangle remote sensing observations to identify and distinguish mineral dust types: 2. Sensitivity over dark water, *J. Geophys. Res.*, *111*, D11207, doi:10.1029/2005JD006756.

Kalashnikova, O. V., R. Kahn, I. N. Sokolik, and W.-H. Li (2005), Ability of multiangle remote sensing observations to identify and distinguish mineral dust types: Optical models and retrievals of optically thick plumes, *J. Geophys. Res.*, *110*, D18S14, doi:10.1029/2004JD004550.

Kaufman, Y. J. (1987), Satellite sensing of aerosol absorption, *J. Geophys. Res.*, *92*, 4307–4317, doi:10.1029/JD092iD04p04307.

Kaufman, Y. J., C. J. Tucker, and I. Fung (1990), Satellite measurements of large-scale air pollution: Methods, *J. Geophys. Res.*, *95*, 9927–9939, doi:10.1029/JD095iD07p09927.

Kaufman, Y. J., D. Tanré, O. Dubovik, A. Karnieli, and L. A. Remer (2001), Absorption of sunlight by dust as inferred from satellite and ground-based remote sensing, *Geophys. Res. Lett.*, *28*, 1479–1482, doi:10.1029/2000GL012647.

Kaufman, Y. J., D. Tanré, and O. Boucher (2002), A satellite view of aerosols in the climate system, *Nature*, *419*, 215–223, doi:10.1038/nature01091.

Koren, I., Y. J. Kaufman, L. A. Remer, and J. V. Martins (2004), Measurements of the effect of Amazon smoke on inhibition of cloud formation, *Science*, *303*, 1342–1345, doi:10.1126/science.1089424.

Koren, I., J. V. Martins, L. A. Remer, and H. Afargan (2008), Smoke invigoration versus inhibition of clouds over the Amazon, *Science*, *321*, 946–949, doi:10.1126/science.1159185.

Maignan, F., F.-M. Breon, and R. Lacaze (2004), Bidirectional reflectance of Earth targets: Evaluation of analytical models using a large set of spaceborne measurements with emphasis on the hot spot, *Remote Sens. Environ.*, *90*, 210–220, doi:10.1016/j.rse.2003.12.006.

Martins, J. V., P. Artaxo, C. Liousse, J. S. Reid, P. V. Hobbs, and Y. J. Kaufman (1998), Effects of black carbon content, particle size, and mixing on light absorption by aerosols from biomass burning in Brazil, *J. Geophys. Res.*, *103*, 32,041–32,050, doi:10.1029/98JD02593.

Martins, J. V., D. Tanré, L. Remer, Y. Kaufman, S. Mattoo, and R. Levy (2002), MODIS Cloud screening for remote sensing of aerosols over oceans using spatial variability, *Geophys. Res. Lett.*, *29*(12), 8009, doi:10.1029/2001GL013252.

Martins, J. V., P. Artaxo, Y. J. Kaufman, A. D. Castanho, and L. A. Remer (2009), Spectral absorption properties of aerosol particles from 350–2500 nm, *Geophys. Res. Lett.*, *36*, L13810, doi:10.1029/2009GL037435.

McComiskey, A., S. E. Schwartz, B. Schmid, H. Guan, E. R. Lewis, P. Ricchiazzi, and J. A. Ogren (2008), Direct aerosol forcing: Calculation from observables and sensitivities to inputs, *J. Geophys. Res.*, *113*, D09202, doi:10.1029/2007JD009170.

Menon, S., J. Hansen, L. Nazarenko, and Y. Luo (2002), Climate effects of black carbon aerosols in China and India, *Science*, *297*, 2250–2253, doi:10.1126/science.1075159.

Mishchenko, M. I., et al. (2007), Accurate monitoring of terrestrial aerosols and total solar irradiance—Introducing the Glory Mission, *Bull. Am. Meteorol. Soc.*, *88*, 677–691.

Mitchell, J. M., Jr. (1971), The effect of atmospheric aerosols on climate with special reference to temperature near Earth's surface, *J. Appl. Meteorol.*, *10*, 703–714, doi:10.1175/1520-0450(1971)010<0703:TEOAAO>2.0.CO;2.

Moosmüller, H., P. K. Chakrabarty, and W. P. Arnott (2009), Aerosol absorption and its measurement: A review, *J. Quant. Spectrosc. Radiat. Transfer*, *110*, 844–878, doi:10.1016/j.jqsrt.2009.02.035.

Penner, J. E., E. R. Dickinson, and A. C. O'Neill (1992), Effects of aerosol from biomass burning on the global radiation budget, *Science*, *256*, 1432–1434, doi:10.1126/science.256.5062.1432.

Procopio, A. S., P. Artaxo, Y. J. Kaufman, L. A. Remer, J. S. Schafer, and B. N. Holben (2004), Multilayer analysis of Amazonian biomass burning smoke radiative forcing of climate, *Geophys. Res. Lett.*, *31*, L03108, doi:10.1029/2003GL018646.

Ramana, M. V., and V. Ramanathan (2006), Abrupt transition from natural to anthropogenic aerosol radiative forcing: Observations at the ABC-Maldives Climate Observatory, *J. Geophys. Res.*, *111*, D20207, doi:10.1029/2006JD007063.

Ramanathan, V., P. J. Crutzen, J. T. Kiehl, and D. Rosenfeld (2001), Aerosols, climate, and the hydrological cycle, *Science*, *294*, 2119–2124, doi:10.1126/science.1064034.

Ramanathan, V., et al. (2005), Atmospheric brown clouds: Impacts on South Asian climate and hydrological cycle, *Proc. Natl. Acad. Sci. U. S. A.*, *102*, 5326–5333, doi:10.1073/pnas.0500656102.

Ramanathan, V., et al. (2007), Warming trends in Asia amplified by brown cloud solar absorption, *Nature*, *448*, 575–578, doi:10.1038/nature06019.

Reid, J. S., P. V. Hobbs, C. Liousse, J. V. Martins, R. E. Weiss, and T. F. Eck (1998), Comparisons of techniques for measuring shortwave absorption and black carbon content of aerosols from biomass burning in Brazil, *J. Geophys. Res.*, *103*, 32,031–32,040, doi:10.1029/98JD00773.

Ricchiazzi, P., S. Yang, C. Gautier, and D. Sowle (1998), SBDART: A research and Teaching software tool for plane-parallel radiative transfer in the Earth's atmosphere, *Bull. Am. Meteorol. Soc.*, *79*, 2101–2114, doi:10.1175/1520-0477(1998)079<2101:SARATS>2.0.CO;2.

Satheesh, S. K., et al. (2009), Improved assessment of aerosol absorption using OMI-MODIS joint retrieval, *J. Geophys. Res.*, *114*, D05209, doi:10.1029/2008JD011024.

Sato, M., et al. (2003), Global atmospheric black carbon inferred from AERONET, *Proc. Natl. Acad. Sci. U. S. A.*, *100*, 6319–6324, doi:10.1073/pnas.0731897100.

Torres, O., P. K. Bhartia, J. R. Herman, Z. Ahmad, and J. Gleason (1998), Derivation of aerosol properties from satellite measurements of backscattered ultraviolet radiation: Theoretical basis, *J. Geophys. Res.*, *103*, 17,099–17,110, doi:10.1029/98JD00900.

Wang, C. (2004), A modeling study on the climate impacts of black carbon aerosols, *J. Geophys. Res.*, *109*, D03106, doi:10.1029/2003JD004084.

Wiscombe, W. J. (1980), Improved Mie scattering algorithm, *Appl. Opt.*, *19*, 1505–1509, doi:10.1364/AO.19.001505.

Zaveri, R. A., J. C. Barnard, R. C. Easter, N. Riemer, and M. West (2010), Particle-resolved simulation of aerosol size, composition, mixing state, and the associated optical and cloud condensation nuclei activation properties in an evolving urban plume, *J. Geophys. Res.*, *115*, D17210, doi:10.1029/2009JD013616.

Zhu, A., V. Ramanathan, F. Li, and D. Kim (2007), Dust plumes over the Pacific, Indian, and Atlantic oceans: Climatology and radiative impact, *J. Geophys. Res.*, *112*, D16208, doi:10.1029/2007JD008427.

J. V. Martins and L. Zhu, Department of Physics, Joint Center for Earth Systems Technology, University of Maryland, Baltimore County, 1000 Hilltop Circle, Baltimore, MD 21250, USA. (martins@umbc.edu; zhuli1@umbc.edu)

L. A. Remer, NASA Goddard Space Flight Center, Code 613.2, Greenbelt, MD 20771, USA. (Lorraine.A.Remer@nasa.gov)